

Adsorption of selenium(VI) onto nano transition alumina

Jordan, N.; Franzen, C.; Lützenkirchen, J.; Foerstendorf, H.; Hering, D.; Weiss, S.;
Heim, K.; Brendler, V.;

Originally published:

June 2018

Environmental Science: Nano 5(2018)7, 1661-1669

DOI: <https://doi.org/10.1039/c8en00293b>

Perma-Link to Publication Repository of HZDR:

<https://www.hzdr.de/publications/Publ-27204>

Release of the secondary publication
on the basis of the German Copyright Law § 38 Section 4.

Uptake of selenium(VI) onto nano transition alumina

Norbert Jordan^{1,*}, Carola Franzen¹, Johannes Lützenkirchen², Harald Foerstendorf¹,
David Hering^{1,3}, Stephan Weiss¹, Karsten Heim¹, Vinzenz Brendler¹

¹Helmholtz-Zentrum Dresden - Rossendorf (HZDR), Institute of Resource Ecology, Bautzner
Landstraße 400, 01328 Dresden (Germany)

²Institute for Nuclear Waste Disposal, Karlsruhe Institute of Technology, Hermann-von-
Helmholtz Platz 1, 76344 Eggenstein-Leopoldshafen (Germany)

³current affiliation: sunfire GmbH

Gasanstaltstraße 2, 01237 Dresden, Germany

*Corresponding author:

Phone: +49 351 260 2148, e-mail: n.jordan@hzdr.de

Abstract

The adsorption of selenium(VI) onto nano transition alumina (γ/δ -Al₂O₃) was investigated at both macroscopic and molecular levels. The uptake of selenium(VI) was found to decrease upon increasing pH (5-10) and ionic strength (0.01-0.1 mol·L⁻¹). At the molecular level, *in situ* attenuated total reflection Fourier-transform infrared (ATR FT-IR) spectroscopy established the predominant formation of a bidentate outer-sphere surface complex throughout the investigated pH range. The acid-base surface properties of transition alumina (surface charge) together with the Se(VI) adsorption edges were successfully described using a 1-pK with charge distribution surface complexation model and one outer-sphere surface species, namely $\{(\equiv\text{AlOH}_2^{+0.5})_2\text{SeO}_4^{2-}\}$, according to the IR studies. These new spectroscopic results can be implemented in reactive transport models to enable a more consistent and trustworthy prognostic modeling of the environmental fate of selenium(VI).

KEYWORDS: Selenium(VI); transition alumina; sorption; *in situ* ATR FT-IR spectroscopy; surface complexation modeling

Introduction

Selenium is an essential element with toxic effects when high concentrations ($>400 \mu\text{g}\cdot\text{d}^{-1}$) of bioaccessible species are incorporated.^{1, 2} Mines, coal-fired power plants, oil refineries, and agriculture are important sources of anthropogenic Se dissemination, generating contaminated waters and wastewaters.^{3, 4} Selenium is a potential pollutant of water bodies, its concentration has to be monitored in drinking-water and in wastewaters. Besides its potential chemotoxicity, the ^{79}Se isotope is also an important issue, since it contributes to the radiation inventory of a potential nuclear waste repository due to its long half-life ($\sim 3.27 \times 10^5$ years).⁵ Detailed knowledge about selenium speciation and the resulting mobility and bioavailability is therefore of great importance for both the treatment of Se-contaminated wastewater and the safe disposal of radioactive waste.

Selenate (Se(VI)O_4^{2-}) is the predominant aqueous species under most natural redox conditions.^{1, 2} One major process controlling the mobility of selenium in the environment is the adsorption onto mineral surfaces. Aluminum oxides are among the most abundant and reactive minerals found in soils and sediments.⁶ In addition, they are widely involved in the industry, e.g. for catalytic processes⁷⁻⁹ due to their high surface area. Aluminum oxides have been traditionally used as model oxides to understand the reactivity of clay minerals, since their aluminol surface groups exhibit similar behavior compared to those at the edges of clays.¹⁰ They have also been used in laser-induced luminescence spectroscopy studies as analogues for iron oxides.^{11, 12}

At the macroscopic level, the adsorption of selenium(VI) by $\gamma\text{-Al}_2\text{O}_3$, $\delta\text{-Al}_2\text{O}_3$, gibbsite and aluminum hydroxide has been investigated.^{6, 13-20} For the geochemical modeling of adsorption processes occurring at the water-mineral interface via surface complexation models (SCMs), a comprehensive knowledge derived from spectroscopic investigations on the surface speciation is

mandatory. The formation of non-protonated outer-sphere surface complexes during selenium(VI) sorption onto γ - Al_2O_3 (pH range 4-7), onto hydrous aluminum oxide (pH range 3.5-6.0) and onto hydrated γ - Al_2O_3 surface (pH range 4-7.6) was evidenced by IR, Raman, and EXAFS spectroscopy.^{6, 16, 21} Though the presence of a small fraction of inner-sphere complexes onto γ - Al_2O_3 at pH < 6 was detected,²¹ it was only suggested on hydrous aluminum oxide (pH range 3.5-6).¹⁶

Few studies dealing with surface complexation modeling of selenate adsorption on alumina phases are currently available in the literature, based on the diffuse layer model²² and the triple layer model^{15, 23}. Ghosh et al.²³ considered the two surface species $\{\equiv\text{AlOH}_2^+-\text{HSeO}_4^-\}$ and $\{\equiv\text{AlOH}_2^+-\text{SeO}_4^{2-}\}$, Wu et al.¹⁵ only $\{\equiv\text{AlOH}_2^+-\text{SeO}_4^{2-}\}$, while Wang et al.²² proposed the three species $\{\equiv\text{AlOH}_2-\text{SeO}_4\}^-$, $\{\equiv\text{AlOH}_2-\text{H}_2\text{SeO}_4\}^+$ and $\{\equiv(\text{AlO})_2-\text{SeO}_4\}^{4-}$. None of them constrained the number of species as well as their denticity by spectroscopic evidence. It thus appears that an accurate description of selenium(VI) adsorption on alumina phases via SCMs is currently missing.

The goal of this study was to provide a thorough understanding of the adsorption mechanism of Se(VI) onto nano transition alumina. The thermodynamically stable phase of alumina is α - Al_2O_3 , and other polymorphs such as γ -, δ -, and η - are metastable and usually designed as transition alumina. The oxides are less stable than oxyhydroxides or hydroxides. As a consequence, the surface and bulk properties of the adsorbent have to be controlled, which was achieved in the present work by combining X-ray diffraction (XRD), potentiometric titrations and zeta potential measurements. The macroscopic modelling requires batch sorption data, recorded under different pH, ionic strength and initial Se(VI) concentration conditions. The thermodynamic based description of sorption processes at the solid-water interface based on SCMs has to rely on a

79 thorough description of the number of species at the surface, their stoichiometry and denticity,
80 their binding strength as well as their reversibility. This can be achieved by applying advanced
81 spectroscopic techniques such as attenuated total reflection Fourier-transform infrared (ATR FT-
82 IR) spectroscopy. Indeed, the latter provides a detailed knowledge at the molecular level of the
83 structure of the surface species and permits to follow *in situ* adsorption processes within the sub-
84 minute range, even for micro-molar concentration ranges. Exactly this comprehensive
85 combination of methods was exploited in this study.

86

Experimental

Reagents

The background electrolyte NaCl solutions were prepared from a Merck powder (p.a.) in deionized water (Milli-Q, 18.2 M Ω ·cm). Selenium(VI) stock solutions (0.1 mol·L⁻¹) were prepared by dissolving Na₂SeO₄ (Sigma Aldrich, p.a.) in deionized water (Milli-Q, 18.2 M Ω ·cm). All experiments were carried out using diluted fractions of these solutions and CO₂-free deionized water. In order to avoid possible contamination of the solutions by silicate, and in parallel to minimize container wall adsorption, polypropylene or polycarbonate flasks were used in all experiments.

Characterization of nano transition Al₂O₃

Al₂O₃ was purchased from Alfa Aesar (No. 44931, 99.5 % purity specified by the supplier). The particle size ranges between 40 and 50 nm according to the manufacturer. The specific surface area (SSA) was determined to be 37 m²·g⁻¹ by the Brunauer–Emmet–Teller (BET) equation with nitrogen adsorption isotherms at 77 K (Multi-point Beckman Coulter analyzer SA 3100). Minor impurities of approx. 20 μ g·g⁻¹ for Mg, Cu, and W, 120 μ g·g⁻¹ for Fe and 550 μ g·g⁻¹ for Ca were observed by inductively coupled plasma-mass spectrometry (ICP-MS, ELAN 9000 Perkin Elmer) after digestion of the mineral. XRD measurements revealed the presence of both γ -Al₂O₃ (ICDD 00–002–1420) and δ -Al₂O₃ (ICDD 00–056–1186) in a ratio of approximately 30:70 (Figure S1, Supporting Information (SI)). No detectable impurities (> 5 % w/w) of other aluminum phases such as e.g. gibbsite or bayerite were observed in the raw material.

In order to check potential phase transformation of transition- Al_2O_3 , samples (mass to volume ratio $m/v = 0.5 \text{ g}\cdot\text{L}^{-1}$) were suspended in $0.1 \text{ mol}\cdot\text{L}^{-1}$ NaCl aqueous solutions with pH values ranging from 4 to 12 (adjusted with 0.1 and $0.01 \text{ mol}\cdot\text{L}^{-1}$ HCl and NaOH), in a glove box under anoxic conditions (N_2 atmosphere, $\text{O}_2 < 10 \text{ ppm}$). The pH measurements (pH-meter Inolab WTW series pH720) were performed using a combination glass electrode (BlueLine 16 pH, Schott Instruments) with a Ag/AgCl reference electrode, to an accuracy of ± 0.05 . Electrodes were calibrated using three NIST-traceable buffer solutions from WTW (pH 1.679, pH 4.006 and pH 6.865, each value for 25°C). After 16 days of equilibration at room temperature with regular pH adjustment, the samples were centrifuged and subsequently lyophilized. Afterwards the samples were also characterized by XRD. Additionally, the solubility of transition- Al_2O_3 was checked on the same samples ($m/v = 0.5 \text{ g}\cdot\text{L}^{-1}$, 16 days of shaking, $0.1 \text{ mol}\cdot\text{L}^{-1}$ NaCl). For this, the supernatants of the batch experiments after phase separation were analyzed by ICP-MS in order to derive the concentration of dissolved aluminum.

The impact of pH (from 3.5 to 11), and duration of mineral ageing in suspension (one hour to four weeks) on the zeta potential of transition alumina ($m/v = 0.2 \text{ g}\cdot\text{L}^{-1}$, $0.1 \text{ mol}\cdot\text{L}^{-1}$ NaCl) was evaluated at 25°C using a Laser-Doppler-Electrophoresis instrument (nano-ZS, Malvern Instruments Ltd.). The results are shown in Figure S2 in the SI.

The surface acid-base properties of nano transition alumina were characterized by potentiometric titrations and zeta potential studies. Potentiometric titrations (pH range 5 to 9.5) were performed at different ionic strengths of NaCl (0.1 , 0.05 and $0.01 \text{ mol}\cdot\text{L}^{-1}$) with a Metrohm 736 GP Titrino titrator, at a mass to volume ratio of $30 \text{ g}\cdot\text{L}^{-1}$ under Ar atmosphere (SI). This high solid to liquid ratio minimizes the effects of solubility relative to the surface reactions. Zeta

potential measurements were performed under CO₂ exclusion, at $m/v = 0.25 \text{ g}\cdot\text{L}^{-1}$ and at two ionic strengths (0.005 and $0.01 \text{ mol}\cdot\text{L}^{-1}$ NaCl).

Batch Sorption experiments

The impact of pH and ionic strength on the sorption of Se(VI) onto alumina was studied in the pH range from 5 to 10 at room temperature. The mass to volume ratio was 0.5 or $1 \text{ g}\cdot\text{L}^{-1}$. All sorption experiments were performed in a glove box under anoxic conditions (N₂ atmosphere, O₂ < 10 ppm). The suspensions were equilibrated for 3 days in a head-over-head shaker (with pH adjustment). Required amounts of selenium(VI) were added to reach a concentration of $1 \times 10^{-5} \text{ mol}\cdot\text{L}^{-1}$ or $2 \times 10^{-5} \text{ mol}\cdot\text{L}^{-1}$ and the suspensions were shaken for 2 more days, which made sure that constant uptake was achieved, since a time-dependent study (data not shown) indicated a plateau of the sorption process reached after a contact time of less than 24 h. pH measurements were performed as already described above. At the end of the sorption stage, the samples were centrifuged at $12,000 \times g$ for 2 h (Sigma 3-30KH centrifuge). Scattered light intensity measurements (BI-90 particle sizer, Brookhaven Instruments) were used to ensure that supernatants were free of colloids. The selenium concentration in the supernatant, determined by ICP-MS, was used to calculate the amount of adsorbed selenium(VI). Se uptake on the walls of polypropylene vials was found to be negligible. Additionally, zeta potential measurements were performed under CO₂-exclusion, using a m/v of $0.25 \text{ g}\cdot\text{L}^{-1}$, an ionic strength of $0.01 \text{ mol}\cdot\text{L}^{-1}$ and an initial Se(VI) concentration of $1 \times 10^{-4} \text{ mol}\cdot\text{L}^{-1}$.

IR Spectroscopy

The IR experiments were carried out with a Bruker Vertex 80/v spectrometer, equipped with a horizontal ATR diamond crystal accessory (SamplIR II, Smiths Inc., 9 reflections, angle of

incidence: 45°) and a Mercury Cadmium Telluride (MCT) detector. Each IR spectrum was an average over 256 scans at a spectral resolution of 4 cm⁻¹ using the OPUSTM software for data acquisition and evaluation.

The sample compartment was purged with dry air. To minimize interferences between the strong absorption band of H₂O below 1000 cm⁻¹ and the potential SeO₄²⁻ bands arising from adsorption (between 900 and 700 cm⁻¹), all studies were performed in D₂O. All solutions were prepared and measured in N₂ atmosphere to prevent CO₂ interference and fast exchange between hydrogen and deuterium. The pH of the selenium working solution, measured using electrodes calibrated with aqueous buffers as described above, was adjusted with 0.1 mol L⁻¹ NaOD and DCl. pD values were then calculated from pH values using the equation pD = pH + 0.4.²⁴ The determination of the selenium sorption mechanisms onto transition alumina was analogous to earlier spectroscopic adsorption studies.²⁵⁻²⁸

Briefly, transition alumina was deposited directly on the surface of the diamond crystal from a 2.5 g·L⁻¹ suspension and dried under a gentle N₂ flow. As a first step, for equilibration of the mineral film, the cell was rinsed with the background electrolyte (0.1 and 0.01 mol·L⁻¹ NaCl) for 60 minutes. Transition alumina might provide spectral interferences during the investigation of Se(VI) adsorption processes, since significant bands between 1000 and 600 cm⁻¹ are present (Figure S3 in SI). However, experiments in the presence of the background electrolyte clearly evidenced the long-term stability of the transition alumina on the ATR cell. Then, the blank electrolyte solution was replaced by the selenium(VI) solution (5 × 10⁻ mol·L⁻¹) for 2 hours, to study the adsorption processes. As a last step, the film was rinsed again with a blank solution for 60 minutes to study the potential desorption of selenium(VI) from the transition alumina film. All steps were performed with solutions at constant pD and involved a continuous flow rate of

100 $\mu\text{L}\cdot\text{min}^{-1}$ provided by a peristaltic pump. Acquisition of single beam spectra was continuously accomplished during all steps of the experiment. Spectra reflecting the molecular processes occurring at the solid-liquid interface were calculated from the single beam spectra before and during each experimental step according to Lambert-Beer's law.

Surface Complexation Modeling

Surface complexation modeling was performed using the charge distribution-multi site complexation (CD-MUSIC) model with a one-pK approach. To describe the surface properties of transition alumina, the pragmatic approach used by Mayordomo et al.²⁸ was followed. One site representing singly coordinated hydroxyl groups with fractional charges was used, involving a site density of 7 sites·nm⁻². A pK of 9.3 was used to model the potentiometric titrations and zeta potential measurements data. A better data description was achieved with the three plane model in comparison to the Basic Stern model. The adjustable parameters were the two electrolyte association constants (Na^+ and Cl^- , located at the head-end of the diffuse layer) and the capacitance value C_1 (C_2 being fixed at 5 F·m⁻²).^{28, 29} The slip-plane distance, s , was fitted to obtain a good fit to the zeta potential data.³⁰ The fitting procedure was performed using a modified version of FITEQL coupled to UCODE.^{31, 32} All activity coefficient treatment was done using the Davies equation.

Results and discussion

Surface Acid–base Behavior, Zeta Potentials, and Modeling in the absence of selenate

Several previous studies have shown that γ -Al₂O₃ in aqueous suspensions transforms into (oxy)hydroxides even at room temperature and after a few days.³³⁻³⁷ The pH dependent investigation of the stability of the bulk transition–Al₂O₃ by means of XRD shows that during the equilibration time of 16 days, no transformation to other aluminum-(oxy)-hydroxides, such as boehmite, gibbsite or bayerite took place (Figure 1A). IR data did not reveal any surface transformation of nano transition alumina into bayerite or gibbsite even after 1 month. This observation is in excellent agreement with a previous study by Müller et al.³⁸ who used exactly the same charge.

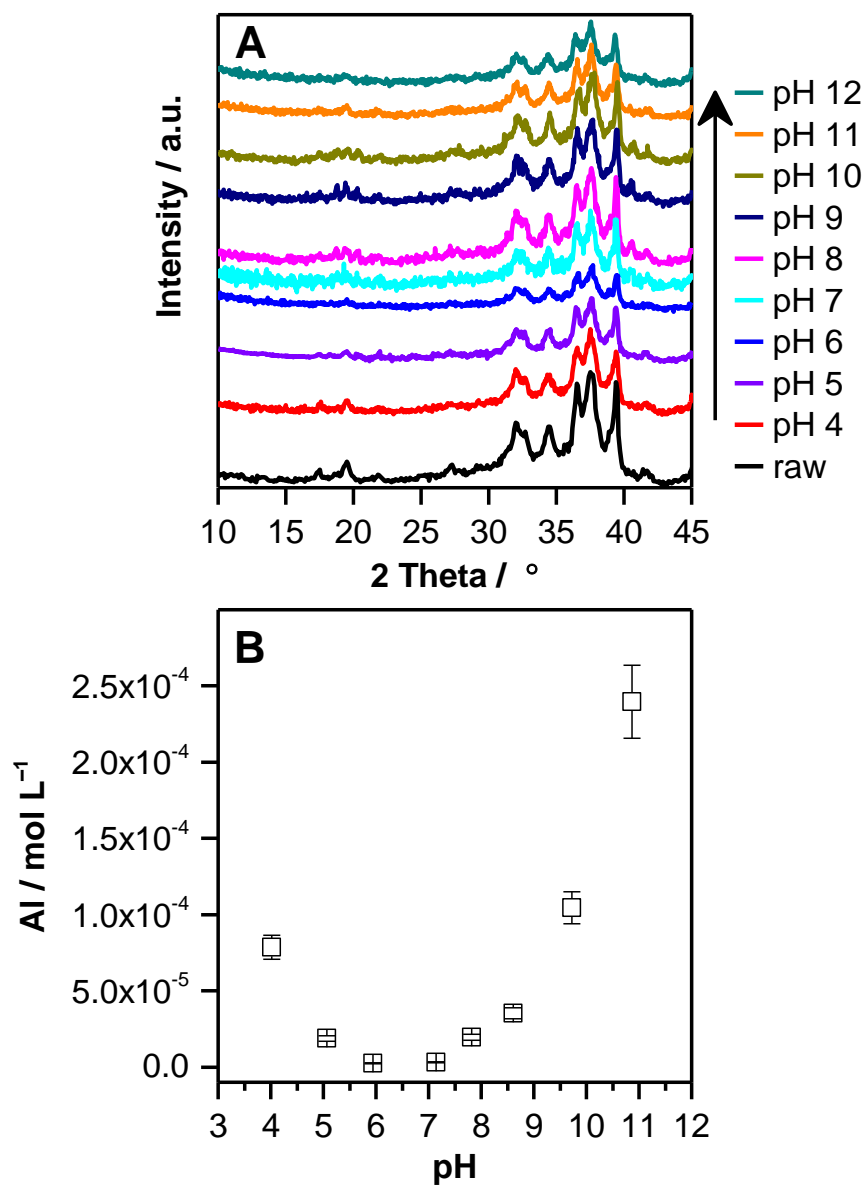


Figure 1. (A) XRD of transition alumina as a function of pH after 16 days of equilibration at room temperature (B) solubility of transition alumina as a function of pH at room temperature (m/v = 0.5 g·L⁻¹, 16 days of shaking, 0.1 mol·L⁻¹ NaCl).

The isoelectric point of transition alumina at 25 °C and 0.1 mol·L⁻¹ NaCl was found at pH 9.5 (Figure S2 in SI) irrespective of different equilibration times ranging from a couple of minutes to four weeks. This value is in good agreement with literature data of γ -Al₂O₃,³⁹ whereas no

literature exists for δ -Al₂O₃. These findings suggest that the variable surface charge does not significantly change, which would rule out ageing processes, in agreement with the spectroscopic results.

The solubility of nano transition alumina was found to increase significantly at pH < 5 and at pH > 9 (Figure 1B). In order to avoid significant dissolution, batch and zeta potential experiments were performed from pH 5 to 10. At pH 9-10, Se uptake becomes negligible and is therefore not impacted by the increased solubility.

Self-consistent modeling of the Se(VI) adsorption data requires the knowledge of the acid-base parameters of the sorbing phase. The experimental titration results (surface charge density vs. pH) at different ionic strengths are shown in Figure 2A, while zeta potential measurements as a function of pH are given in Figure 2B. Solid lines represent the modeling results in each figure.

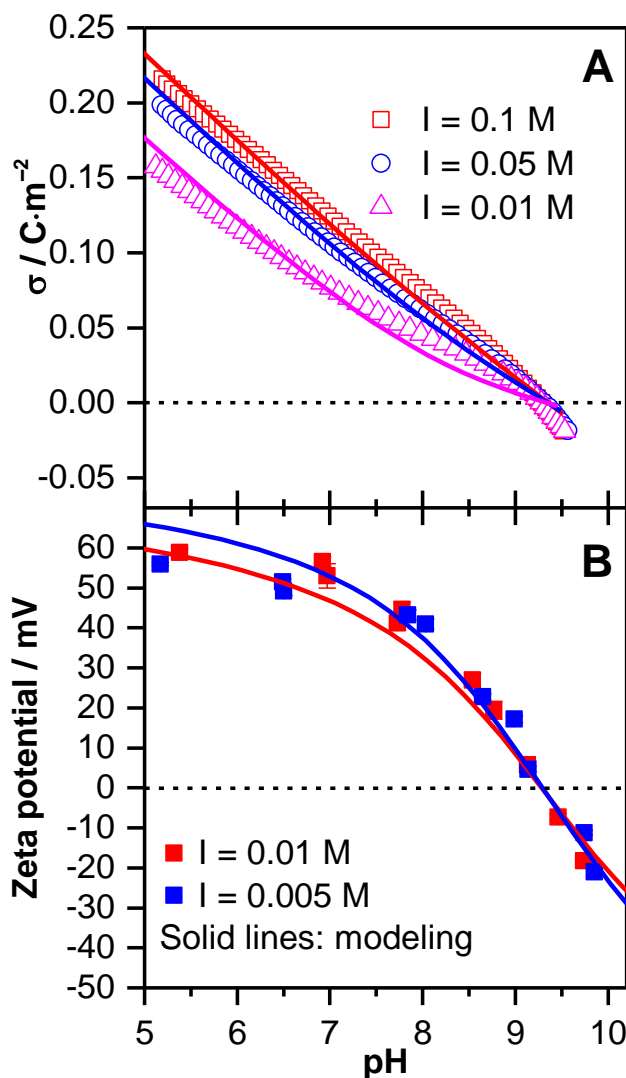


Figure 2. (A) Surface charge of the neat surface of transition alumina ($m/v = 30 \text{ g} \cdot \text{L}^{-1}$, $I = 0.01$, 0.05 and $0.1 \text{ mol} \cdot \text{L}^{-1}$ NaCl, under Ar) (Δ , \circ , \square experiment; — fit). (B) Zeta potential of the neat surface of transition alumina ($m/v = 0.25 \text{ g} \cdot \text{L}^{-1}$, $I = 0.005$ and $0.01 \text{ mol} \cdot \text{L}^{-1}$ NaCl), under N_2 (\blacksquare experiment; — fit).

The surface chemical reactions used and the corresponding constants and required parameters are summarized in Table 1. The capacitance C_I and the parameter x were $1.60 \text{ F} \cdot \text{m}^{-2}$ and 0.33,

respectively. The fitted parameter x is related to the slip plane distance s and the ionic strength dependent Debye length κ by $x = s \times \kappa$.⁴⁰

Table 1. Parameters for the surface species in the Best-Fit Model (surface acid-base properties of nano transition alumina and Se(VI) adsorption).

Surface species	Δz_0	Δz_1	Δz_2	reaction	log K°
Surface acid-base properties					
$\equiv\text{AlOH}^{-0.5}$	0	0	0		0
$\equiv\text{AlOH}_2^{+0.5}$	1	0	0	$\equiv\text{AlOH}^{-0.5} + \text{H}^+ \rightleftharpoons \equiv\text{AlOH}_2^{+0.5}$	9.3
$\equiv\text{AlOH}^{-0.5}\cdots\text{Na}^+$	0	0	1	$\equiv\text{AlOH}^{-0.5} + \text{Na}^+ \rightleftharpoons \equiv\text{AlOH}^{-0.5}\cdots\text{Na}^+$	-0.3 ± 0.2
$\equiv\text{AlOH}^{+0.5}\cdots\text{Cl}^-$	0	0	-1	$\equiv\text{AlOH}_2^{+0.5} + \text{Cl}^- \rightleftharpoons \equiv\text{AlOH}_2^{+0.5}\cdots\text{Cl}^-$	-0.2 ± 0.1
Se(VI) adsorption					
$\{(\equiv\text{AlOH}_2^{+0.5})_2\text{SeO}_4^{2-}\}$	2	-1.7	-0.3	$2(\equiv\text{AlOH}^{-0.5}) + 2\text{H}^+ + \text{SeO}_4^{2-} \rightleftharpoons \{(\equiv\text{AlOH}_2^{+0.5})_2\text{SeO}_4^{2-}\}$	19.5 ± 1.0

The titration data can be satisfactorily described with the proposed model, i.e. with one singly coordinated surface hydroxyl group and the three plane model (Figure 2A). The pH_{IEP} of nano transition alumina was found to be 9.3 and was independent of the NaCl concentration (Figure 2B). This pH_{IEP} value is in agreement with the literature, with $\text{pH}_{\text{PZC/IEP}}$ of alumina phases mostly ranging from pH 8 to 10.^{41, 42} The zeta potential curves and the pH_{IEP} were rather well described by the proposed model (Figure 2B). Charge penetration of the electrolyte ions in the plane 0 or 1 did not significantly improve the quality of both titration and zeta potential fits (i.e. at $I = 0.01 \text{ mol}\cdot\text{L}^{-1}$ in the circumneutral pH range for the titrations and in the pH range from 5 to 7 for

the zeta potentials). The model used to calculate the lines in Figure 2 was consequently accepted and applied for the modeling of the Se(IV) adsorption data.

Batch and zeta potential studies in the presence of selenate

Batch experiments demonstrated that the adsorption of selenium(VI) onto transition alumina was strongly pH-dependent, highest at pH 5 and decreasing with increasing pH (Figure 3A).

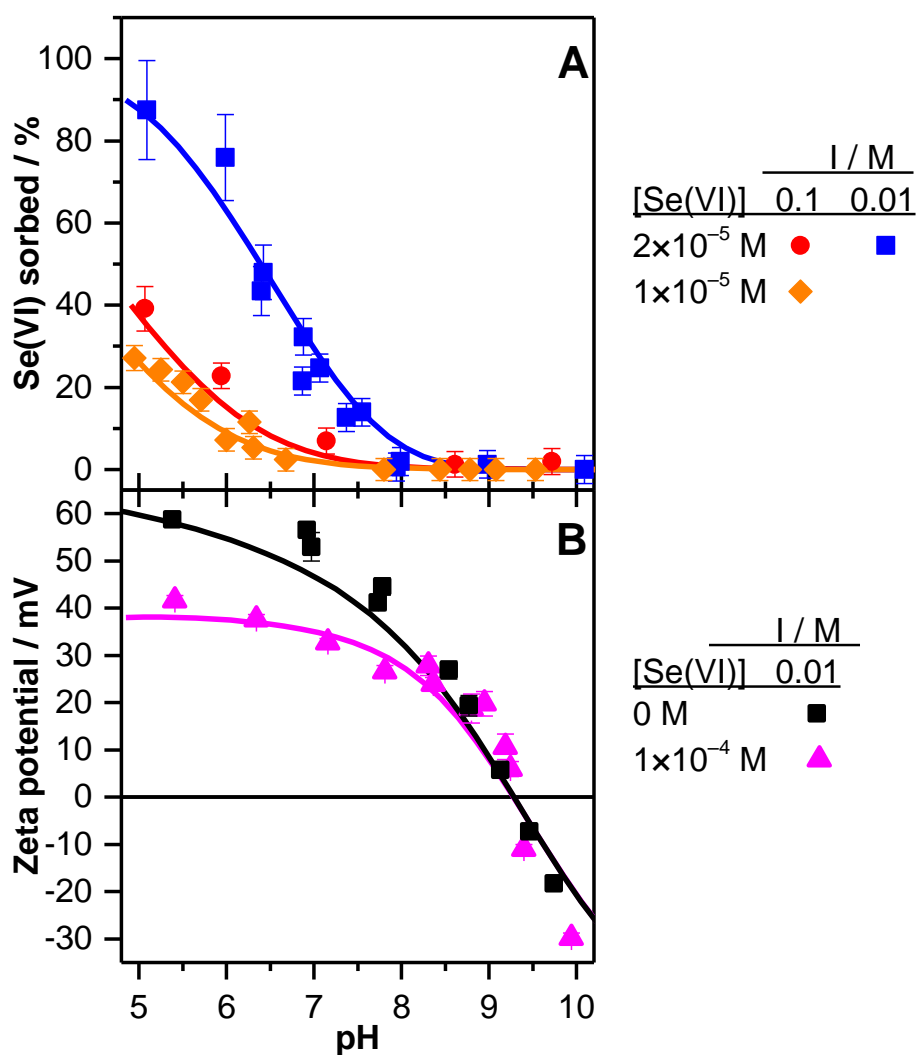


Figure 3. (A) Se(VI) sorption envelopes onto transition alumina ($[\text{Se}^{\text{VI}}]_{\text{initial}} = 1 \times 10^{-5} \text{ mol}\cdot\text{L}^{-1}$, $m/v = 0.5 \text{ g}\cdot\text{L}^{-1}$, $I = 0.1 \text{ mol}\cdot\text{L}^{-1}$ NaCl (♦)) and $[\text{Se}^{\text{VI}}]_{\text{initial}} = 2 \times 10^{-5} \text{ mol}\cdot\text{L}^{-1}$, $m/v = 1 \text{ g}\cdot\text{L}^{-1}$, $I = 0.1 \text{ mol}\cdot\text{L}^{-1}$ NaCl (●) and $I = 0.01 \text{ mol}\cdot\text{L}^{-1}$ NaCl (■); — fit). (B) Zeta potential of the surface of transition alumina ($[\text{Se}^{\text{VI}}]_{\text{initial}} = 0 \text{ mol}\cdot\text{L}^{-1}$ (■) and $1 \times 10^{-4} \text{ mol}\cdot\text{L}^{-1}$ (▲), $m/v = 0.25 \text{ g}\cdot\text{L}^{-1}$, $0.01 \text{ mol}\cdot\text{L}^{-1}$ NaCl). (— fit).

This behavior was expected taking into account (i) that the surface charge of transition alumina decreased with increasing pH and (ii) that selenium(VI) in solution predominantly exists as negatively charged oxyanions. Increasing the ionic strength from 0.01 to $0.1 \text{ mol}\cdot\text{L}^{-1}$ significantly reduced the adsorption of Se(VI), indicating competition with background electrolyte ions and/or electrostatic effects, suggesting the formation of outer-sphere complexes.^{6, 25, 27} From pH 5 to 9, the dissolution of alumina was negligible. Indeed, the Al concentration measured in the supernatants after the phase separation was not exceeding 5.5 % of the concentration corresponding to a theoretical complete dissolution of the sorbing phase. It reached a maximum of 14.5 % between pH 9 and 10, but in this pH range the uptake of Se(VI) was already negligible.

Upon adsorption of Se(VI), the isoelectric point of transition alumina remained unchanged (Figure 3B). However, its zeta potential became less positive at $\text{pH} < \text{pH}_{\text{IEP}}$. A similar behavior of the pH_{IEP} upon selenium(VI) sorption has been previously reported for $\gamma\text{-Al}_2\text{O}_3$,⁶ anatase,²⁵ and maghemite,²⁷ strongly suggesting the formation of outer-sphere complexes.

***In situ* ATR FT-IR studies**

Though solubility experiments revealed increased solubility at $\text{pH} < 5$, the *in situ* IR sorption experiments were performed at pD 4, 5 and 6 to check potential changes in the adsorption mechanism with increasing pH/pD (Figure 4).

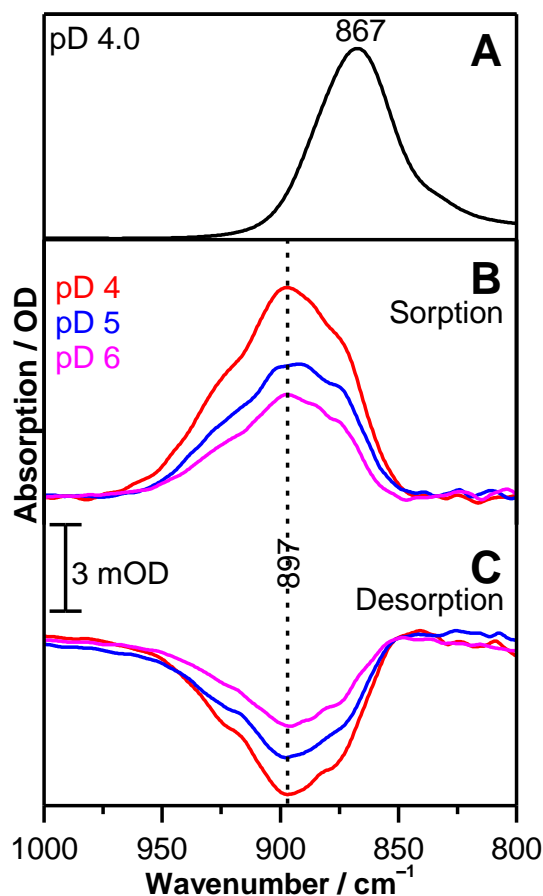


Figure 4. (a) IR spectrum of 0.1 mol·L⁻¹ selenium(VI) in aqueous solution at 0.1 mol·L⁻¹ NaCl in D₂O. (b) *In situ* IR spectra taken during selenium(VI) adsorption onto transition alumina ([Se(VI)]_{initial} = 5 × 10⁻⁴ mol·L⁻¹, D₂O, 0.1 mol·L⁻¹ NaCl, N₂) recorded after 20 minutes of induced sorption at different pD values. (c) *In situ* IR spectra during release of selenium(VI) recorded 20 minutes after starting to flush the transition alumina phase with blank solution (D₂O, 0.1 mol·L⁻¹ NaCl, N₂) at different pD values.

It was shown that a steady state was achieved within 20 minutes since prolonged exposure to Se(VI) up to 120 minutes did not reveal any significant spectral changes (Figures S4, S5 and S6 in SI).

Generally, the amplitudes of the spectra decreased with increasing pD, correlating with the observations from the batch experiments that the Se(VI) uptake decreases with increasing pH/pD (Figure 3A). Furthermore, in analogy to the batch experiments, the decrease of Se(VI) sorption upon increasing the ionic strength from 0.01 to 0.1 mol·L⁻¹ was spectroscopically exemplarily reproduced at pD 4 (Figure S7B in SI). Above pD 6, the acquisition of spectra with a reasonable signal-to-noise ratio became difficult due to the reduced sorption of Se(VI) in this pH range (see Figure 3A).

The interpretation of the vibrational spectra refers to the correlation between the molecule symmetry and the vibrational modes observed. The tetrahedral SeO₄²⁻ anion as it is prevailing in aqueous solution exhibits two IR active modes, the ν_3 triply degenerate asymmetric Se–O stretching and the ν_4 triply degenerate out of plane O–Se–O bending modes.^{43, 44} Since the latter mode is outside the acquisition range of the MCT detector, only the spectral properties of the ν_3 mode are considered. In the spectrum of the aqueous SeO₄²⁻ ion, a single almost symmetrically shaped band at 867 cm⁻¹ is observed reflecting the predominant tetrahedral symmetry of the aqueous SeO₄²⁻ ion (Figure 4A). In contrast, the spectra recorded at pD 4.0, 5.0, and 6.0 after 20 minutes of induced adsorption showed a broad structured band with a maximum around 897 cm⁻¹ indicating the occurrence of overlapping bands (Figure 4B).

The elucidation of the spectral components contributing to these spectra was achieved by second derivative spectra. For the spectrum recorded at pD 4, four spectral components were determined with maxima at 926, 900, 887, and 872 cm⁻¹. The fitting result provided a local residual root-mean-square error ranging from 5.4×10^{-5} to 9.0×10^{-5} (Figure 5A-C).

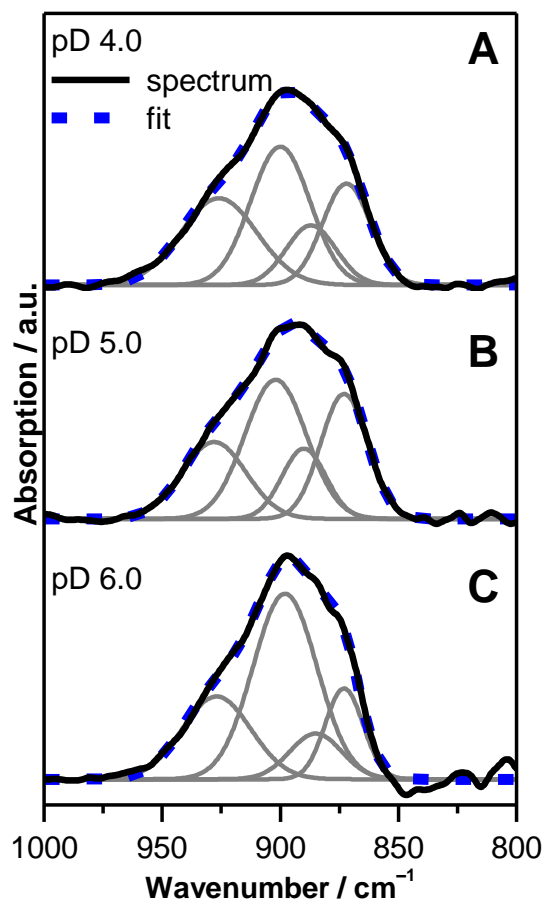


Figure 5. Deconvolution of the IR spectrum of selenium(VI) sorption onto transition alumina ($[\text{Se(VI)}]_{\text{initial}} = 5 \times 10^{-4} \text{ mol}\cdot\text{L}^{-1}$, D_2O , $0.1 \text{ mol}\cdot\text{L}^{-1} \text{ NaCl}$, 20 min of sorption, N_2). Dotted line indicates the overall fit. (a) pD 4.0, (b) pD 5.0 (c) pD 6.0.

Similar fitting results with only marginally varied frequencies of the peak maxima were obtained for the spectra recorded at pD 5 and 6 (Figure 5 B; C) indicating the predominant formation of one type of sorption complex on the transition alumina surface throughout this pD range.

The splitting of the band representing the $\nu_3(\text{SeO}_4)$ mode into four spectral components can be interpreted in terms of the reduction of the molecule symmetry from tetrahedral to C_{2v} as it was previously observed in our investigation of the sorption processes of Se(VI) onto maghemite.²⁷ Intrinsically, lowering the molecule symmetry from T_d to C_{2v} leads to the abrogation of the triply degenerated ν_3 mode. Additionally, the ν_1 mode becomes IR active.²⁷ Hence, the appearance of four spectral components in the IR spectra of the sorption species strongly suggests the prevalence of a surface complex showing C_{2v} symmetry.

Subsequently, desorption was initiated by flushing the flow cell with blank electrolyte solution. The shapes of spectra exhibited a high congruence to the spectra of the sorption step strongly suggesting that the same Se(VI) surface species were present during adsorption and release from the transition alumina surface (Figure 4C). The predominant formation of outer-sphere complexes can be inferred from the high degree of reversibility over time observed by *in situ* ATR FT-IR which ranged from ~67 % to ~76 % from pD 4 to 6, as it was observed for other mineral phases.^{25, 27} Additionally, this is in agreement with the results from our batch and zeta potential experiments (see above). Furthermore, in analogy to the batch experiments, the decrease of Se(VI) sorption upon increasing the ionic strength from 0.01 to 0.1 mol·L⁻¹ was spectroscopically reproduced (Figure S7 in SI). The same spectral characteristics were observed at pD 4.0 at both 0.1 mol·L⁻¹ and 0.01 mol·L⁻¹ NaCl ionic strengths (Figure S7 in SI). In summary, the vibrational spectroscopic findings clearly demonstrated that selenium(VI) sorption onto transition alumina proceeds via the predominant formation of bidentate outer-sphere complexes over the whole pH range investigated.

Surface complexation modeling of Se(VI) adsorption processes

The parameters derived from the acid-base model were kept for the Se(VI)-adsorption model, implying that the inner and outer-layer capacitances were assumed not to be impacted by the adsorption of Se(VI), as well as the slip plane distance. The aqueous Se(VI) protonation constant at infinite dilution were taken from the NEA-TDB book for selenium.⁴⁵ Only the reaction given below is the most relevant for our conditions.



The formation of one bidentate outer-sphere surface species was derived from the spectroscopic studies and implemented in the adsorption model, i.e. $\{(\equiv\text{AlOH}_2^{+0.5})_2\text{SeO}_4^{2-}\}$ (see Table 1). The appropriate formulation of the mass action expression for this bidentate complex was performed according to previous recommendations,^{46, 47} i.e. by decoupling the mole balance and mass balance equations (coefficient 2 only in the matrix B). The location of the charge of the Se(VI) ions at the interface was described via the charge distribution (CD) factor. Overall, two adjustable parameters were involved: the log K and the concomitant CD-factor. The CD-factors can be inferred from Table 1.

The adsorption model is summarized in the following reaction equation and the model fit to the batch and zeta potential data is shown in Figure 3 (A and B).



A satisfactory description of the adsorption data was obtained (Figure 3A), whatever the initial concentration of Se(VI) or the ionic strength of the suspensions. The model description of the zeta potentials of transition alumina in the absence and presence of Se(VI) is shown in Figure 3B. Overall, the description of the zeta potentials is accurate and the model nicely reproduces the absence of a pH_{IEP} shift.

The location of the Se(VI) charge at the interface was characterized by the best-fit charge distribution factor. The CD-factor describes how the negative charge of the selenate ion is distributed in the interfacial layer, i.e. which contribution is going to the 1-plane and the 2-plane. Most of the charge of the SeO_4^{2-} ion is transferred towards the plane 1, leading to a closer position of the selenate ion to the surface compared to the background electrolyte ions. The free SeO_4^{2-} anion has a tetrahedral symmetry and exhibits a bidentate symmetry at the transition alumina water interface. It is thus conceivable that one of the two remaining oxygens is located rather close to the surface and one rather oriented towards the solution.

The model used to calculate the lines in Figure 3 (A and B) and considering the $(\equiv\text{AlOH}_2^{+0.5})_2$ $(\text{SeO}_4)^{2-}$ species was the one that yielded the best fit. Since it describes the experimental data accurately and was in agreement with the spectroscopic observations, other modeling options (sodium coadsorption, another inner-sphere surface species) were not tested. The published SCMs studies for Se(VI) adsorption onto alumina involved different stoichiometry and mechanisms, which makes a direct comparison not suitable.

Conclusions

In this study, the adsorption of Se(VI) on transition alumina was shown to decrease upon increasing pH and ionic strength, leading to a higher Se(VI) mobility under such conditions. At the molecular level, *in situ* ATR FT-IR spectroscopy identified an outer-spheric bidentate surface complex as the predominant interfacial Se species over the whole investigated pH range. The acid-base surface properties as well as the Se(VI) adsorption processes could be successfully described using a 1-pK model with charge distribution, considering one single species as inferred from the IR studies. The data derived from this study will be implemented into a sorption database which is mandatory for safety assessments and for the prediction of Se(VI) fate in the environment. The evidenced outer-sphere adsorption mechanism associated to fast kinetics and high reversibility would lead to Se(VI) retardation. However, the lack of irreversibility of the adsorption process might not be sufficient for preventing Se(VI) leaching and transport in the environment. If bound to nano alumina as a carrier, filtration or adhesion of the nano particles would mean that selenate can be re-mobilized, unlike irreversibly bound inner-sphere surface complexes.

Conflicts of interest

The authors declare no competing financial interest.

Acknowledgements

This work is part of the VESPA project, funded by the German Federal Ministry of Economics and Technology (BMWi) through contract number 02E10790. The authors would like to thank Aline Chlupka and Stefanie Schubert for ICP-MS measurements, Carola Eckardt for BET determination, Heidrun Neubert for titration experiments as well as Andrea Scholz for XRD measurements.

References

1. A. Fernández-Martínez and L. Charlet, *Rev. Environ. Sci. Biotechnol.*, 2009, **8**, 81-110.
2. F. Fordyce, *Ambio*, 2007, **36**, 94-97.
3. M. Navarro-Alarcon and C. Cabrera-Vique, *Science of the Total Environment*, 2008, **400**, 115-141.
4. S. Santos, G. Ungureanu, R. Boaventura and C. Botelho, *Science of the Total Environment*, 2015, **521-522**, 246-260.
5. G. Jörg, R. Buhnemann, S. Hollas, N. Kivel, K. Kossert, S. Van Winckel and C. L. V. Gostomski, *Applied Radiation and Isotopes*, 2010, **68**, 2339-2351.
6. E. J. Elzinga, Y. Z. Tang, J. McDonald, S. DeSisto and R. J. Reeder, *Journal of Colloid and Interface Science*, 2009, **340**, 153-159.
7. D. Laurenti, P. N. Bo, C. Roukoss, E. Devers, K. Marchand, L. Massin, L. Lemaitre, C. Legens, A. A. Quoineaud and M. Vrinat, *Journal of Catalysis*, 2013, **297**, 165-175.
8. M. Trueba and S. P. Trasatti, *European Journal of Inorganic Chemistry*, 2005, DOI: 10.1002/ejic.200500348, 3393-3403.
9. S. Koneti, L. Roiban, A.-S. Gay, P. Avenier, F. Dalmas and T. Epicier, *Microscopy and Microanalysis*, 2016, **22**, 58-59.
10. G. Lagaly and I. Dékány, in *Handbook of Clay Science*, Elsevier, Amsterdam, The Netherlands, Second edn., 2013, ch. 8.
11. T. Rabung, D. Schild, H. Geckeis, R. Klenze and T. Fanghänel, *Journal of Physical Chemistry B*, 2004, **108**, 17160-17165.
12. T. Kupcik, T. Rabung, J. Lützenkirchen, N. Finck, H. Geckeis and T. Fanghänel, *Journal of Colloid and Interface Science*, 2016, **461**, 215-224.
13. J. S. Yamani, A. W. Lounsbury and J. B. Zimmerman, *Water Research*, 2014, **50**, 373-381.
14. N. Loffredo, S. Mounier, Y. Thiry and F. Coppin, *Journal of Environmental Radioactivity*, 2011, **102**, 843-851.
15. C. H. Wu, S. L. Lo and C. F. Lin, *Colloids and Surfaces a-Physicochemical and Engineering Aspects*, 2000, **166**, 251-259.
16. D. Peak, *Journal of Colloid and Interface Science*, 2006, **303**, 337-345.
17. J. A. Ippolito, K. G. Scheckel and K. A. Barbarick, *Journal of Colloid and Interface Science*, 2009, **338**, 48-55.
18. C. P. Schulthess and Z. Q. Hu, *Soil Science Society of America Journal*, 2001, **65**, 710-718.
19. E. J. Boyle-Wight, L. E. Katz and K. F. Hayes, *Environmental Science & Technology*, 2002, **36**, 1212-1218.
20. S. Goldberg, *Soil Science Society of America Journal*, 2014, **78**, 473-479.
21. H. Wijnja and C. P. Schulthess, *Journal of Colloid and Interface Science*, 2000, **229**, 286-297.
22. P. M. Wang, A. Anderko and D. R. Turner, *Industrial & Engineering Chemistry Research*, 2001, **40**, 4444-4455.
23. M. M. Ghosh, C. D. Cox and J. R. Yuanpan, *Environmental Progress*, 1994, **13**, 79-88.
24. P. K. Glasoe and F. A. Long, *Journal of Physical Chemistry*, 1960, **64**, 188-190.
25. N. Jordan, H. Foerstendorf, S. Weiss, K. Heim, D. Schild and V. Brendler, *Geochimica et Cosmochimica Acta*, 2011, **75**, 1519-1530.

26. N. Jordan, K. Muller, C. Franzen and V. Brendler, *Journal of Colloid and Interface Science*, 2013, **390**, 170-175.
27. N. Jordan, A. Ritter, H. Foerstendorf, A. C. Scheinost, S. Weiss, K. Heim, J. Grenzer, A. Mucklich and H. Reuther, *Geochimica et Cosmochimica Acta*, 2013, **103**, 63-75.
28. N. Mayordomo, H. Foerstendorf, J. Lützenkirchen, K. Heim, S. Weiss, U. Alonso, T. Missana, K. Schmeide and N. Jordan, *Environmental Science & Technology*, 2018, **52**, 581-588.
29. T. Hiemstra, H. Yong and W. H. Van Riemsdijk, *Langmuir*, 1999, **15**, 5942-5955.
30. M. Bouby, J. Lützenkirchen, K. Dardenne, T. Preocanin, M. A. Denecke, R. Klenze and H. Geckeis, *Journal of Colloid and Interface Science*, 2010, **350**, 551-561.
31. J. C. Westall, *FITEQL: A Computer Program for Determination of Chemical Equilibrium Constants from Experimental Data*, Department of Chemistry, Oregon State University, Corvallis, OR, U.S.A., 1982.
32. E. P. Poeter and M. C. Hill, *Documentation of UCODE: A Computer Code for Universal Inverse Modeling*, 1998.
33. C. Dyer, P. J. Hendra, W. Forsling and M. Ranheimer, *Spectrochimica Acta Part A: Molecular Spectroscopy*, 1993, **49**, 691-705.
34. E. Laiti, P. Persson and L. O. Öhman, *Langmuir*, 1998, **14**, 825-831.
35. H. Wijnja and C. P. Schulthess, *Spectrochimica Acta Part A: Molecular and Biomolecular Spectroscopy*, 1999, **55**, 861-872.
36. G. Lefèvre, M. Duc, P. Lepeut, R. Caplain and M. Fédoroff, *Langmuir*, 2002, **18**, 7530-7537.
37. X. Carrier, E. Marceau, J. F. Lambert and M. Che, *Journal of Colloid and Interface Science*, 2007, **308**, 429-437.
38. K. Müller, H. Foerstendorf, V. Brendler, A. Rossberg, K. Stolze and A. Gröschel, *Chemical Geology*, 2013, **357**, 75-84.
39. G. Jegadeesan, K. Mondal and S. B. Lalvani, *Environmental Technology*, 2003, **24**, 1049-1059.
40. J. Lützenkirchen, T. Preocanin and N. Kallay, *Physical Chemistry Chemical Physics*, 2008, **10**, 4946-4955.
41. M. Kosmulski, *Surface Charging and Points of Zero Charge*, CRC Press 2009.
42. M. Kosmulski, *Journal of Colloid and Interface Science*, 2011, **353**, 1-15.
43. K. Nakamoto, *Infrared and Raman Spectra of Inorganic and Coordination Compounds. Part A: Theory and Applications in Inorganic Chemistry*, Wiley-Interscience, New York, Fifth edn., 1997.
44. C. M. Su and D. L. Suarez, *Soil Science Society of America Journal*, 2000, **64**, 101-111.
45. A. Olin, B. Nöläng, E. G. Osadchii, L.-O. Öhman and E. Rosén, *Chemical thermodynamics of selenium.*, Elsevier, Amsterdam, 2005.
46. J. Lützenkirchen, R. Marsac, D. A. Kulik, T. E. Payne, Z. R. Xue, S. Orsetti and S. B. Haderlein, *Applied Geochemistry*, 2015, **55**, 128-137.
47. Z. M. Wang and D. E. Giammar, *Environmental Science & Technology*, 2013, **47**, 3982-3996.

SUPPORTING INFORMATION

Uptake of selenium(VI) onto transition alumina

Norbert Jordan^{1,*}, Carola Franzen¹, Johannes Lützenkirchen², Harald Foerstendorf¹,
David Hering³, Stephan Weiss¹, Karsten Heim¹, Vinzenz Brendler¹

¹Helmholtz-Zentrum Dresden - Rossendorf (HZDR), Institute of Resource Ecology, Bautzner
Landstraße 400, 01328 Dresden (Germany)

²Institute for Nuclear Waste Disposal, Karlsruhe Institute of Technology, Hermann-von-
Helmholtz Platz 1, 76344 Eggenstein-Leopoldshafen (Germany)

³current affiliation: sunfire GmbH
Gasanstaltstraße 2, 01237 Dresden, Germany

*Corresponding author:

Phone: +49 351 260 2148, e-mail: n.jordan@hzdr.de

This supporting information contains 11 pages and 7 figures.

XRD of raw transition alumina

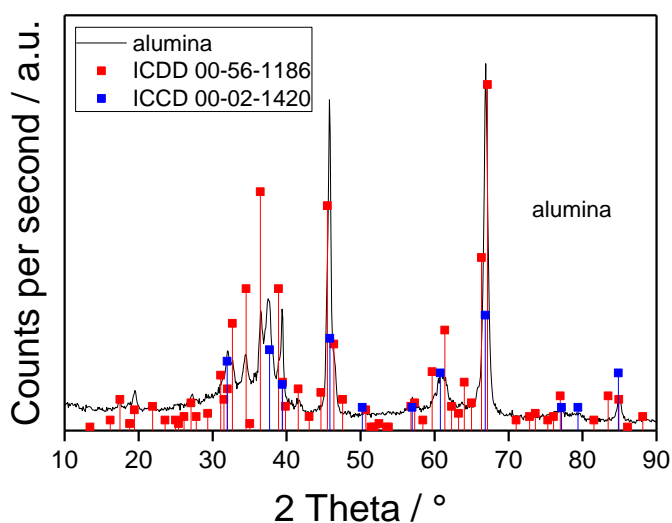


Figure S1. X-ray diffraction pattern of nano transition alumina at room temperature compared with the ICDD cards 00-056-1186 and 00-02-1420.

The Al_2O_3 sample was characterized by XRD on a D8 Bruker-AXS diffractometer equipped with a graphite secondary monochromator, using $\text{Cu K}\alpha$ radiation ($\lambda = 1.5406 \text{ \AA}$) and operating in diffraction mode at 40 kV and 40 mA. Samples were step-scanned in the 2θ range of $20\text{--}90^\circ$ in steps of 0.05° (15 s per step). By comparing the XRD patterns to the International Centre for Diffraction Data (ICDD) cards (Figure S1), the sample was identified as a polycrystalline phase mixture of $\gamma\text{-Al}_2\text{O}_3$ (ICDD 00-002-1420) and $\delta\text{-Al}_2\text{O}_3$ (00-056-1186) in a ratio of approximately 30:70.

Effect of aging on the surface properties of transition- Al_2O_3

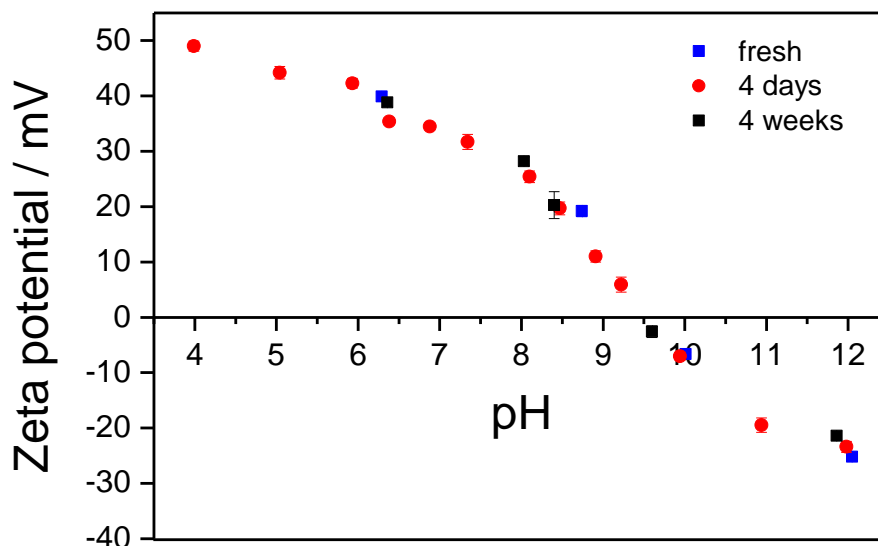


Figure S2. Zeta potential of transition alumina as a function of pH and time at 25 °C (m/v = 0.2 g·L⁻¹, 0.1 mol·L⁻¹ NaCl).

Alumina was suspended in 50 mL polypropylene tubes in the presence of 40 mL of 0.1 mol·L⁻¹ NaCl solution (Merck, p.a.), yielding a mass to volume ratio m/v of 0.2 g·L⁻¹. Samples were prepared in ambient air, since no impact of atmospherically derived carbonate on the zeta potential was observed in preliminary investigations. Suspensions were stirred and the pH values of the oxide suspensions were adjusted using either 0.1 or 0.01 mol·L⁻¹ HCl or NaOH. Each sample was ultrasonicated for 15 s with an ultrasonic finger (Sonopulse HD 2200, Bandelin) prior to measurements. An aliquot of approximately 1 mL was then transferred into a rectangular capillary cell made of polycarbonate with gold plated copper beryllium electrodes. A voltage of 50 V was applied across them. After 2 min of equilibration, the electrophoretic mobility of the suspension was measured at 25 °C. The measured velocity of the particle in the electric field was

converted to zeta potential using the Smoluchowski equation. The zeta potential was calculated with Zetasizer 6.01 software. The reported values were averaged over at least ten measurements.

Potentiometric titrations

Potentiometric titrations (pH range 5 to 9.5) were performed at different ionic strengths of NaCl (0.1, 0.05 and 0.01 mol L⁻¹) with a Metrohm 736 GP Titrino titrator. For each titration, a 30 g L⁻¹ suspension of nano transition alumina (50 mL volume) was inserted in a borosilicate vessel and equilibrated over night at pH ~5. A continuous argon flux (Argon N50 from Air Liquide) was applied over the suspension to minimize intrusion of atmospheric CO₂. To ensure a homogeneous suspension, a Teflon propeller was used. After overnight pre-equilibration, titration by base was performed by addition of aliquots (20 µL) of 0.1 mol L⁻¹ NaOH. The pH electrode (Schott BlueLine 11pH) was calibrated using a three point calibration with buffer solutions (pH 4.01, 6.87 and 9.18).

FT-IR studies

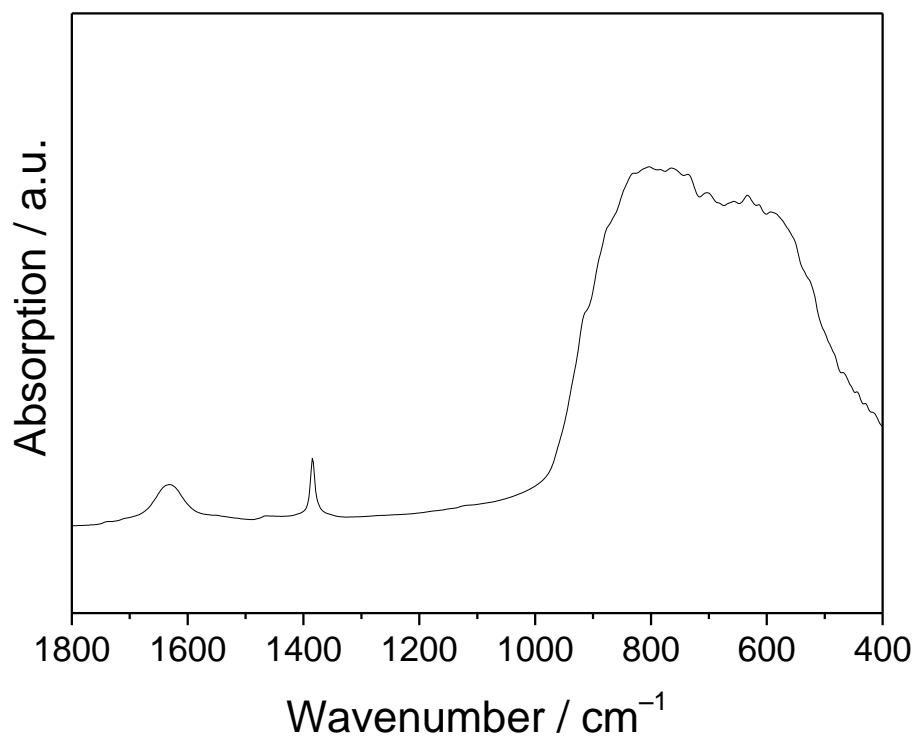


Figure S3. IR spectrum of transition alumina measured in a KBr matrix.

IR spectra of Se(VI) sorption and desorption processes and dependence on ionic strength

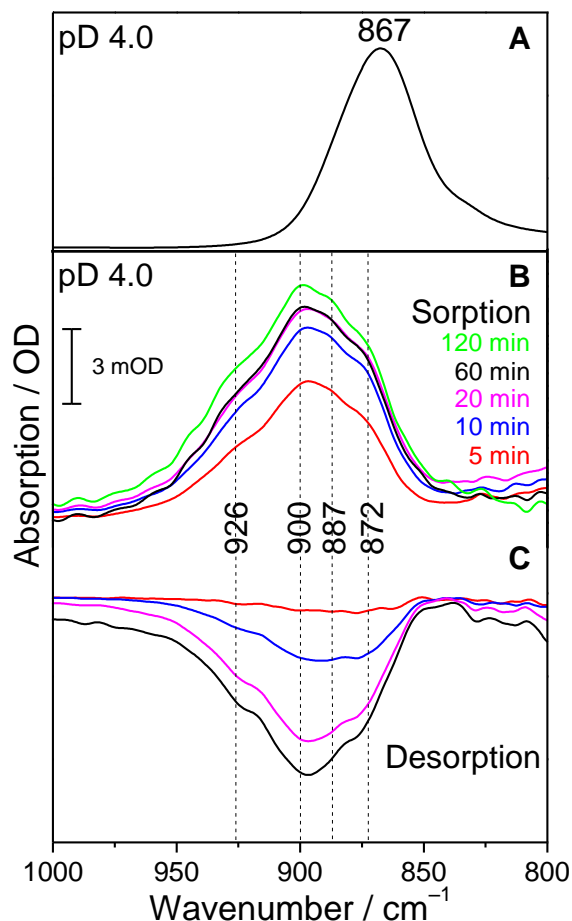


Figure S4. (a) IR spectrum of 0.1 mol L⁻¹ selenium(VI) in aqueous solution at 0.1 mol L⁻¹ NaCl in D₂O. (b) *In situ* IR spectra taken during selenium(VI) adsorption onto transition alumina ([Se(VI)]_{initial} = 5 × 10⁻⁴ mol L⁻¹, D₂O, pD 4.0, 0.1 mol L⁻¹ NaCl, N₂) at different times. (c) *In situ* IR spectra during release of selenium(VI) at different times after starting to flush the transition alumina phase with blank solution (D₂O, pD 4.0, 0.1 mol L⁻¹ NaCl, N₂).

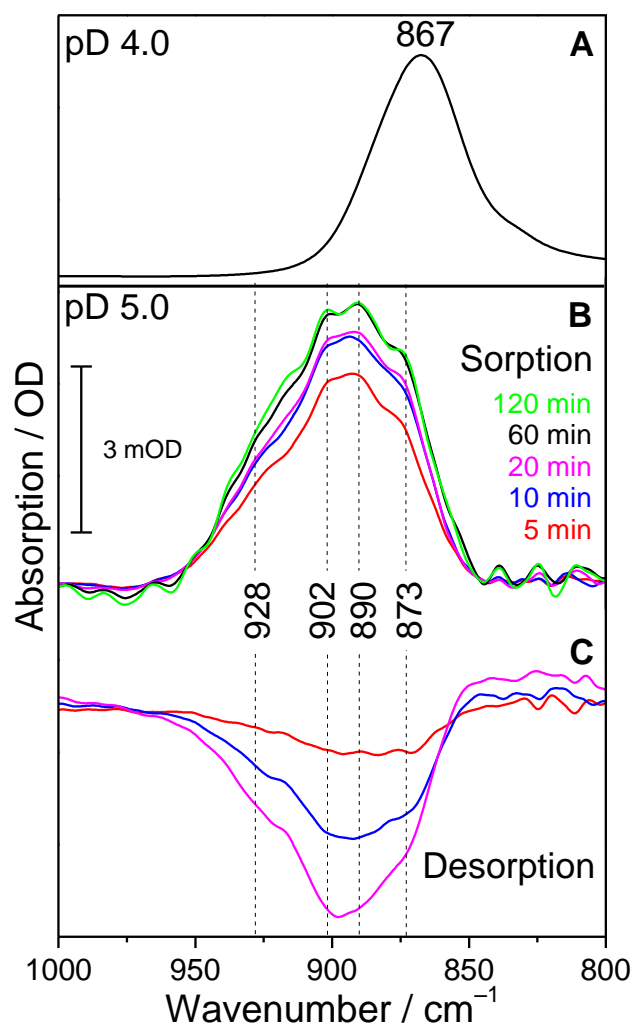


Figure S5. (a) IR spectrum of 0.1 mol L⁻¹ selenium(VI) in aqueous solution at 0.1 mol L⁻¹ NaCl in D₂O. (b) *In situ* IR spectra taken during selenium(VI) adsorption onto transition alumina ([Se(VI)]_{initial} = 5 × 10⁻⁴ mol L⁻¹, D₂O, pD 5.0, 0.1 mol L⁻¹ NaCl, N₂) at different times. (c) *In situ* IR spectra during release of selenium(VI) at different times after starting to flush the transition alumina phase with blank solution (D₂O, pD 5.0, 0.1 mol L⁻¹ NaCl, N₂).

The increase of the amplitudes after 60 minutes of induced sorption (Figure 5b) is only apparent because a continuous background drift occurred throughout the *in situ* experiment. This drift has an almost linear contribution to the spectra's amplitudes with time, thus, becoming obvious with

increasing acquisition time. In fact, already after 20 min the spectra did not show a significant increase of the amplitudes as can be derived from Figures S5c.

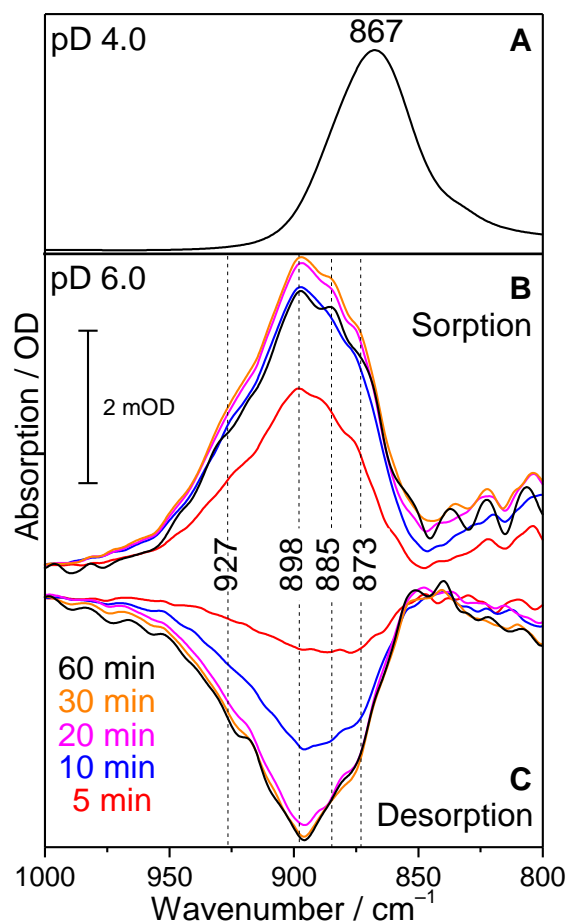


Figure S6. (a) IR spectrum of 0.1 mol L^{-1} selenium(VI) in aqueous solution at 0.1 mol L^{-1} NaCl in D_2O . (b) *In situ* IR spectra taken during selenium(VI) adsorption onto transition alumina ($[\text{Se(VI)}]_{\text{initial}} = 5 \times 10^{-4} \text{ mol L}^{-1}$, D_2O , pD 6.0, 0.1 mol L^{-1} NaCl, N_2) at different times. (c) *In situ* IR spectra during release of selenium(VI) at different times after starting to flush the transition alumina phase with blank solution (D_2O , pD 6.0, 0.1 mol L^{-1} NaCl, N_2).

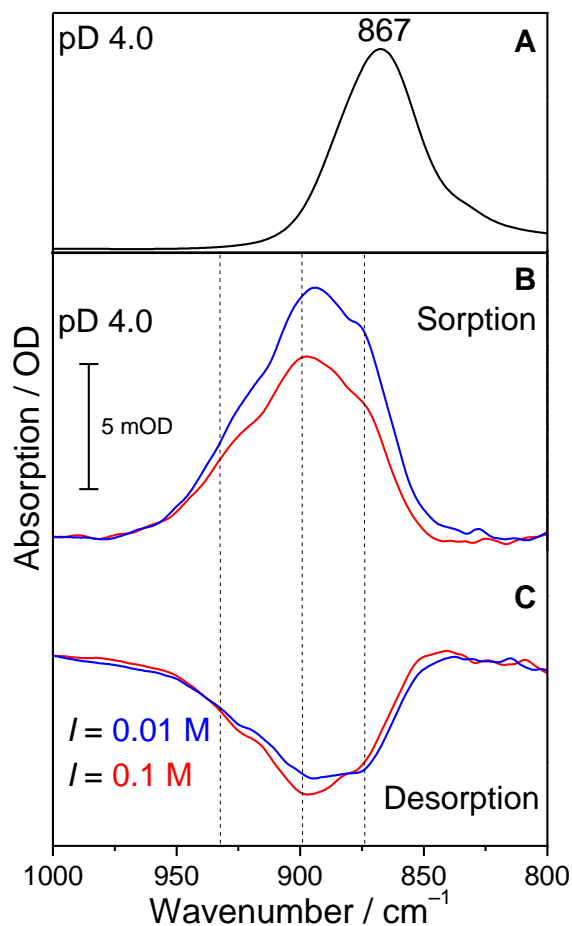


Figure S7. (a) IR spectrum of 0.1 mol L^{-1} selenium(VI) in aqueous solution at 0.1 mol L^{-1} NaCl in D_2O . (b) *In situ* IR spectra taken during selenium(VI) adsorption onto transition alumina ($[\text{Se(VI)}]_{\text{initial}} = 5 \times 10^{-4}\text{ mol L}^{-1}$, D_2O , pD 4, 20 min of sorption, N_2) recorded at different ionic strength. (c) *In situ* IR spectrum of release of selenium(VI) (D_2O , pD 4.0, 20 min of desorption, N_2) recorded at different ionic strength after starting to flush the transition alumina phase with blank solution.